A Broadband DLCZ Quantum Memory in Room-Temperature Atoms

Jian-Peng Dou[†],[1,2] Ai-lin Yang[†],[1,2] Mu-Yan Du,[1] Di Lao,[1] Jun Gao,[1,2] Lu-Feng Qiao,[1,2]
Hang Li,[1,2] Xiao-Ling Pang,[1,2] Zhen Feng,[1,2] Hao Tang,[1,2] and Xian-Min Jin[1,2,*]

[1]*State Key Laboratory of Advanced Optical Communication Systems and Networks, Institute of Natural Sciences & Department of Physics and Astronomy, Shanghai Jiao Tong University, Shanghai 200240, China*

[2]*Synergetic Innovation Center of Quantum Information and Quantum Physics, University of Science and Technology of China, Hefei, Anhui 230026, China*

(Dated: April 24, 2017)

arXiv:1704.06309v1 [quant-ph] 20 Apr 2017

Quantum memory, capable of stopping flying photons and storing their quantum coherence, is essential for scalable quantum technologies. A broadband quantum memory operating at room temperature will enable building large-scale quantum systems for real-life applications, for instance, high-speed quantum repeater for long-distance quantum communication and synchronised multi-photon quantum sources for quantum computing and quantum simulation. Albeit advances of pushing bandwidth from narrowband to broadband and storage media from ultracold atomic gas to room-temperature atomic vapour, due to either intrinsic high noises or short lifetime, it is still challenging to find a room-temperature broadband quantum memory beyond conceptional demonstration. Here, we present a far off-resonance Duan-Lukin-Cirac-Zoller (DLCZ) protocol and for the first time demonstrate a genuine broadband quantum memory that is free of noise and limitation of time bandwidth product in room-temperature atoms. We observed a reported ever lowest unconditional noise level of 0.0001 and a cross-correlation between Stokes photon and anti-Stokes photon up to 28. A measurement of Cauchy-Schwarz inequality yields a violation of 320 standard deviations, which clearly indicates high-fidelity generation and preservation of non-classical correlation in room-temperature atoms. Without using any population preserving technique, we have reached a time bandwidth product up to 1400. Our results pave the avenue towards quantum memory-enabled applications in high speed at ambient condition, especially for scalable quantum communications and quantum computing.

Quantum technologies, incorporating quantum mechanics into communication, information processing and metrology, promise spectacular quantum enhanced advantages beyond what can be done classically [1]. However, quantum states are very fragile and easily get lost to environment, while their generation and quantum operations are mostly probabilistic, which make it exponentially hard to build long-distance quantum channel for quantum communications [2, 3] and large quantum systems for quantum computing [4, 5]. Quantum memory [6] allows quantum states being stored and retrieved in a programmable fashion, therefore provides an elegant solution to the probabilistic nature and associated limitation by coordinating asynchronous events [7–9].

Enormous advances of quantum memory have been made in developing various photon storage protocols and their physical implementations, such as electromagnetically induced transparency [10–12], DLCZ memory [8, 13], off-resonant Faraday interaction [14, 15], controlled reversible inhomogeneous broadening [16–19], atomic frequency combs [20], photon echoes [21–23] and Raman memory [24–26]. In order to have quantum memory practicable for efficient synchronisation and physical scalability, considerable efforts have been dedicated to meet key features known as high efficiency, low noise level, large time bandwidth product (lifetime divided by pulse duration) and operating at room temperature [6].

It has been proven very difficult to satisfy all the requirements simultaneously. Especially in the regime of large bandwidth and room temperature, noise and/or decoherence become dominant and therefore lead to inability of working in quantum regime [27, 28] or only in extremely short time [29, 30]. At room temperature, EIT and near off-resonance Raman memory have a collision-induced fluorescence noise which can not be filtered out because of being identical with signal photons [27]. By applying larger detuning, far off-resonance Raman is found to be able to well eliminate the fluorescence noise and posses a large storage bandwidth. Unfortunately, a new noise rising from spontaneous Raman scattering process becomes dominant, which is intrinsic and proportional to the detuning[28] .

Here we present a far off-resonance DLCZ protocol where we exploit spontaneous Raman scattering process to generate and store an excitation rather than taking it as noise. We demonstrate a genuine broadband quantum memory that can simultaneously meet aforementioned key features. We have observed an unconditional noise level of 0.0001 and a cross-correlation between heralding Stokes photon and retrieved anti-Stokes photon up to 28. A violation of Cauchy-Schwarz inequality [31] up to 320 standard deviations indicates high-fidelity generation and preservation of non-classical correlation in room-temperature atoms. A time bandwidth product of 1400 can be promptly employed to build large-scale quantum networks.

As is shown in Figure 1a, in contrast to "mapping in and out" of external photons in other quantum memory protocols, DLCZ memory creates one collective excitation directly inside of it by a classical write pulse via spontaneous Raman process, meanwhile emits a Stokes photon which can herald

*xianmin.jin@sjtu.edu.cn
†These authors contributed equally.

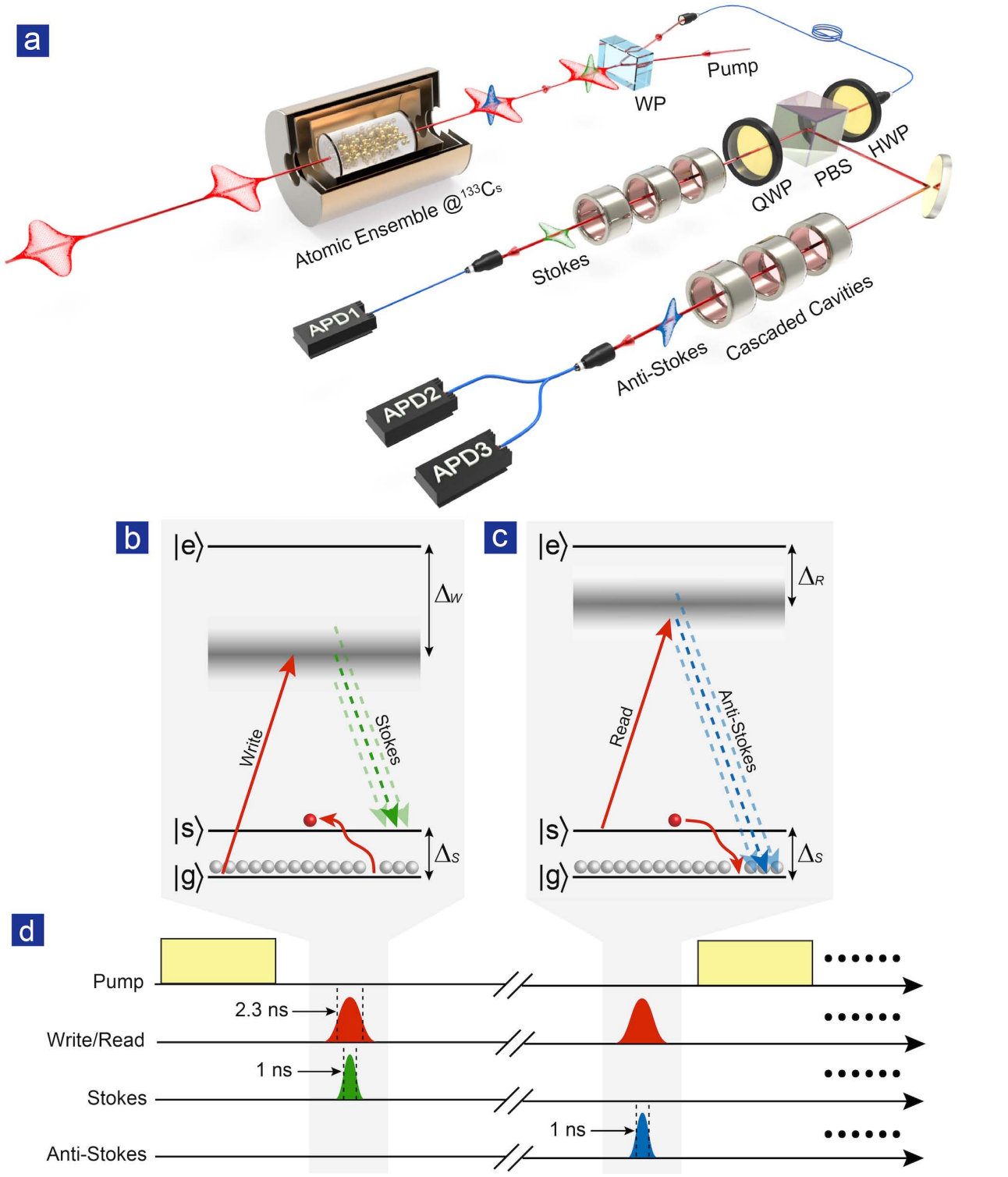

FIG. 1: **Experimental setup and far off-resonance DLCZ scheme**. **a.** The caesium cell is packed in a three-layer magnetic shielding and is heated up to 61.3 °C. The write and read pulses (red envelopes) are generated with a programmed time delay and are both prepared in horizontal polarisation (see Methods). The created Stokes photons (green envelope) and retrieved anti-Stokes photons (blue envelope) are both in vertical polarisation. A Wollaston prism (WP) is employed as polarisation filter to separate the output photons from the write and read pulses. The two sets of cascaded cavities serve as strong spectrum filters and contribute extinction ratio up to 10^7. The colours are only for eye guiding. HWP: half-wave plate, QWP: quarter wave plate, PBS: polarization beam splitter. **b.** The write process of far off-resonance DLCZ quantum memory. The blurred gray belt denotes broadband virtual excited state induced by write pulse. The green dash lines represent wide transition band of a Stokes photon. $\Delta_S = 9.2\,\mathrm{GHz}$ is the ground state hyperfine splitting of caesium. **c.** The read process of far off-resonance DLCZ quantum memory. The blue dash lines represent wide transition band of a anti-Stokes photon.**d.** The time sequence for generation, storage and retrieval of nonclassical correlation. Ellipsis implies repeated sequences afterward.

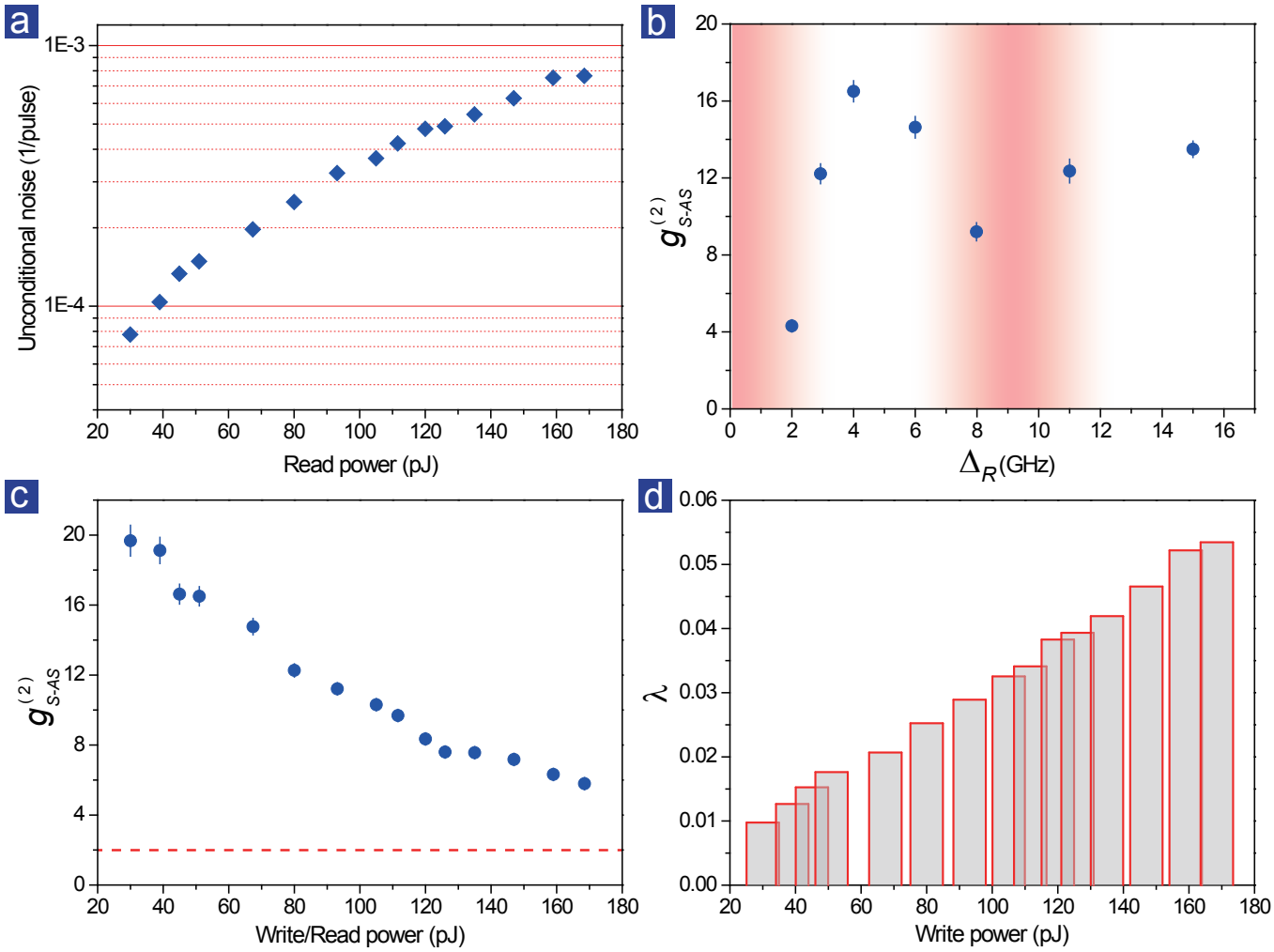

FIG. 2: **Experimental results on the noise level and nonclassicality**. **a.** The measured unconditional noise level as a function of the read power. **b.** The measurement of cross-correlation in a large detuning from near to far off-resonance region, Δ_R from 2 GHz to 15 GHz, correspondingly $\Delta_W = \Delta_R + 9.2\,\mathrm{GHz}$. **c.** Influence of the write/read power, $g^{(2)}_{S\text{-}AS}$ above the boundary (the dash line) implies non-classical correlation. **d.** The relation between excitation probability λ and the write power.

the successful storage with intrinsic unit efficiency[8]. With a programmable delay, a read pulse can retrieve the stored excitation as anti-Stokes photon with a process similar to Raman memory protocol, which has also been demonstrated the potential to approach unit efficiency[25].

By combining far off-resonance atomic configuration and standard DLCZ process, an excited virtual energy level near the two photon resonance can be created by the strong write/read pulse (see Figure 1b, 1c and 1d). The linewidth of the excited virtual energy level is proportional to the intensity of the write/read laser and the effective optical depth of atomic ensemble. In our experiment, we use broadband write and read pulse with pulse duration 2.3 ns and detune them to a very far off-resonance region, Δ_W and Δ_R are larger than 4 GHz and 13.2 GHz respectively, which is about one order higher than narrowband DLCZ quantum memory protocol. We adopt ceasium atoms ^{133}Cs to have large optical depth relying on its high vapour pressure. With 75-mm-long cell and 10 Torr Ne buffer gas, an optical depth 400 is obtained at a temperature of 61.3 °C. The storage bandwidth is expected to be near GHz level and its central frequency is tunable by detuning the write and read pulse either simultaneously or separately.

A simplified three-level Λ-type configuration is illustrated in Figure 1b and 1c, the lower two energy states $|g\rangle\left(6S_{1/2}, F=3\right)$ and $|s\rangle\left(6S_{1/2}, F=4\right)$ are the hyperfine ground states of caesium, and the higher energy state $|e\rangle\left(6P_{3/2}, F'=2,3,4,5\right)$ is the excited state. Initially, a pumping laser resonant with the transition of $6S_{1/2}, F=4 \rightarrow 6P_{3/2}, F'=4\,\mathrm{co}\,5$ prepare all the atoms into the state $|g\rangle$ as

$$|g_1 g_2 \cdots g_N\rangle\,, \tag{1}$$

where N is the total number of atoms participate in interaction. After the initial state is prepared, a strong write pulse with a detuning Δ_W creates a single excitation among millions of atoms meanwhile induce a broadband Stokes photon via spontaneous Raman scattering. In this process, appropri-

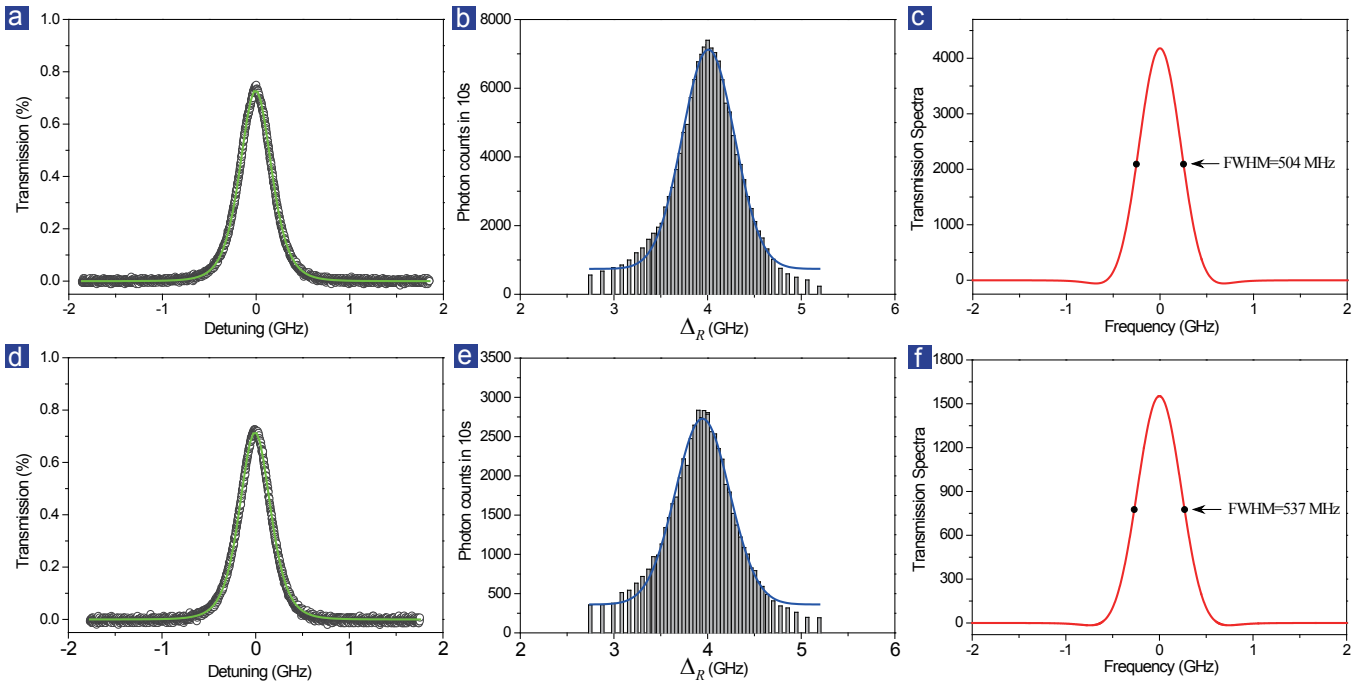

FIG. 3: **Experimental results of convolution-based bandwidth measurement**. We measure the total transmission spectra of cascaded cavities for Stokes (**a**) and anti-Stokes photons (**d**). We then detune the write/read light to get another transmission spectra for Stokes (**b**) and anti-Stokes photons (**e**). We deduce the frequency spectra of Stokes (**c**) and anti-Stokes photons (**f**) by using convolution theorem and Fourier transform.

ate power of the write pulse is adopted to ensure that only a single Stokes photon is emitted per attempt and high-order emission is negligible. Then the collective excitation state can be expressed as[32]

$$\frac{1}{\sqrt{N}}\sum_{n=1}^{N} e^{i(\mathbf{k}_W-\mathbf{k}_S)\mathbf{r}_n}\,|g_1 g_2\cdots g_{n-1}s_n g_{n+1}\cdots g_N\rangle\,, \quad (2)$$

where $\mathbf{k}_W$ is the wave vector of the write pulse, $\mathbf{k}_S$ is the wave vector of the Stokes photon, $\mathbf{r}_n$ is the position of the nth atom. After a programmable delay, a strong read pulse with a detuning Δ_R and wave vector $\mathbf{k}_R$ illuminates the caesium cell and transform the collective excitation into a broadband anti-Stokes photon whose wave vector is denoted by $\mathbf{k}_{AS}$.

The write and read pulse are coaxial, which implies $\mathbf{k}_W = \mathbf{k}_R$, in order to maximise the spin wave lifetime of atomic excitation [34]. It has been theoretically demonstrated that the Stokes photons is mainly inside a small cone around the direction of the write pulse [33]. According to phase-matching condition $\mathbf{k}_W+\mathbf{k}_R = \mathbf{k}_S+\mathbf{k}_{AS}$, we infer the Stokes and anti-Stokes photons are approximately coaxial as well. As shown in Figure 1a, both Stokes and anti-Stokes photons are orthogonal to the write/read pulse [35] and therefore can be separated from the strong addressing light with a high-extinction Wollaston polariser. Two sets of homemade cascaded cavities composed of three Fabry-Perot cavities tuned resonant with Stokes and anti-Stokes photons respectively. Each cavity has a transmission rate about 90% and contribute an extinction ratio more than 500 (see Methods). Together with a polarising beam splitter and a quarter wave plate, we realise a dichroic-mirror-like functioning but for an extremely small frequency difference of 9.2 GHz. A standard Hanbury-Brown and Twiss interferometer composed of three avalanched photodiodes and a 50:50 fibre beamsplitter are employed to perform photon statistics and correlation detection.

Unconditional noise is a key parameter that can be used to benchmark the noise level of optical memory and whether it can work at quantum regime. We retrieve and count anti-Stokes photons in absence of the write pulse. As a result of the novel protocol and experimental configuration, we observe a reported ever lowest unconditional noise level of 0.0001. We obtain a value of $7.79(5)\times10^{-5}$ when we address atoms with the read power of 30 pJ (see Figure 2a). A distinct manifestation of such low unconditional noise level presents as strong nonclassical correlation between heralding Stokes photon and retrieved atomic excitation anti-Stokes photon. It turns out to be a high cross-correlation $g^{(2)}_{S\text{-}AS}$ and a violation of Cauchy-Schwarz inequality $(g^{(2)}_{S\text{-}AS})^2 \leq g^{(2)}_{S\text{-}S}\cdot g^{(2)}_{AS\text{-}AS}$ [31]. We obtain an auto-correlation of $g^{(2)}_{S\text{-}S} = 1.97\pm0.13$ ($g^{(2)}_{AS\text{-}AS} = 1.87\pm0.20$) for Stokes photon (anti-Stokes photon) and cross-correlation of 7.83 ± 0.18, with the detuning Δ_R at 4 GHz, the write/read power 129 pJ and the delay time 30 ns. The Cauchy-Schwarz inequality is violated up to 320 standard deviations, which clearly indicates a high-fidelity generation and preservation of non-classical correlation in our quantum memory.

It is important but technically challenging to investigate

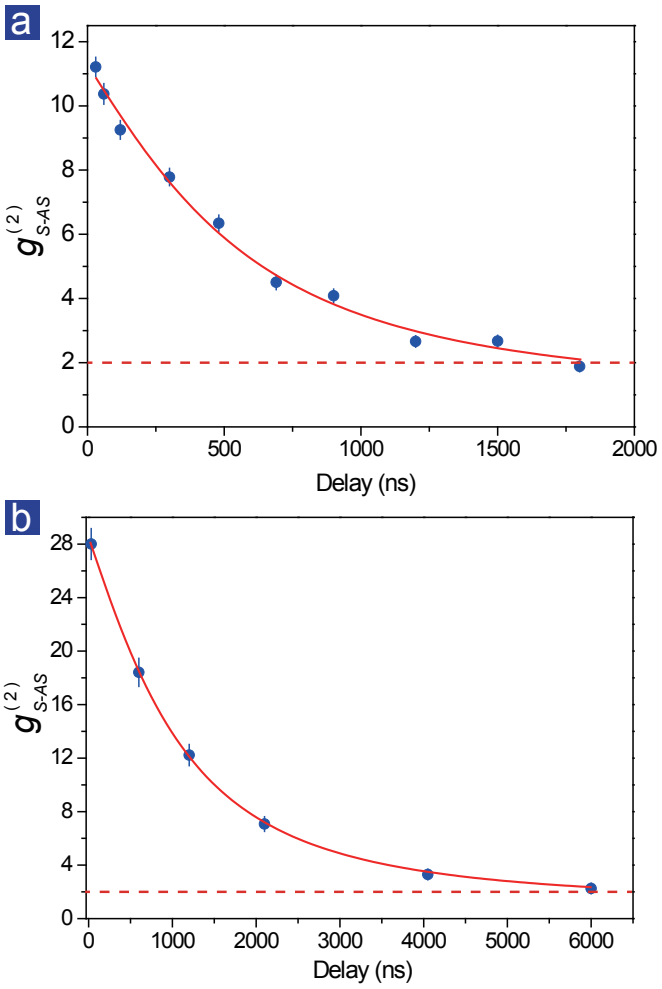

FIG. 4: **Lifetime measurement. a.** The measured cross-correlation as a function of storage time. The data is obtained under the condition of a write/read beam waist of 90 μ m, power about 100 pJ and the detuning $\Delta_R = 4$ GHz. **b.** The observed improvement of lifetime and cross-correlation by expanding the beam waist to 240 μ m. Error bars are derived on the basis of the Poisson distribution of single photon detecters. The red curve is a theoretical fit of the form $g^{(2)}_{S\text{-}AS} = 1 + C/(1 + At^2 + Bt)$.

storage performance depending on detuning of addressing light. For every detuning data point in Figure 2b, we realise this by detuning and locking the write/read frequency far away from the transition line of caesium, and also initialising the resonance for all cascaded cavities. We have made measurement of cross-correlation in a large detuning range Δ_R from 2 GHz to 15 GHz. For broadband optical memory at room temperature, we for the first time identify the performance ranging from near to far off resonance. Our results show a "sweet spot" but in consistent with previous results in narrowband Raman memory experiments which identify 1.3 GHz as optimal detuning[36]. Apart from the detuning around 0 or 9.2 GHz where the leakage of fluorescence through cascaded cavities is not negligible, far-off resonance DLCZ quantum memory shows ability of well working at quantum regime in a wide spectrum. We also made the measurement of cross-correlation and created rate of atomic excitation by scanning the write/read power, which reveals a higher cross-correlation up to 20 at lower excitation rate. (see Figure 2c and 2d).

In order to obtain the bandwidth of our quantum memory, we develop a convolution-based approach (see Methods). We measure the total transmission spectra of cascaded cavities by scanning a narrowband classical light shown in Figure 3a and 3d. We then count Stokes and anti-Stokes photons while scanning the detuning of the write/read light, shown in Figure 3b and 3e. By using convolution theorem and Fourier transform, we can deduce the frequency spectra of Stokes and anti-Stokes photons shown in Figure 3c and 3f. With the write/read power of 96 pJ, the measured bandwidth of Stokes and anti-Stokes photons are 504 MHz and 537 MHz respectively.

Time bandwidth product is the key figure of merit of quantum memory endowed with the capacity of synchronisation. This parameter sets the limit of times that we can synchronise within the lifetime of stored correlations. We measure $g^{(2)}_{S\text{-}AS}$ as a function of storage time, see Figure 4a. The data is fitted with the form $g^{(2)}_{S\text{-}AS} = 1 + C/(1 + At^2 + Bt)$ where At^2 results from atomic random motion [34], and Bt is a correction term that reflects the effect of the background noise. The lifetime is defined with the cross-correlation dropping to 1/e, which is found to reach 800 ns, see Figure 4a. The fitting function reveals our storage time is mainly determined by the time for the atoms propagating through the interaction region. Through enlarging the mode field of both the write/read pulse, we achieve to prolong the lifetime to 1400 ns and obtain a time bandwidth product up to 1400. We also observe a higher cross-correlation of 28 and being higher than 2 until time delay is 6000 ns.

Further promotions of this quantum memory performance can be made for more challenging applications[32]. Our current heralding efficiency conditional on registering a Stokes photon is around 10%, which is obtained by directly dividing correlated photon pair coincidence by Stokes photons counts and total detection efficiency of anti-Stokes photons. This method may underestimate genuine retrieval efficiency and therefore set a lower bound. However, we would like not to derive a retrieval efficiency by subtracting noise and mismatched part, since the heralding efficiency reflects real capacity of quantum memory in terms of applications.

In the light of the fact that the off-resonance Raman process has been proven to be able to reach unit retrieval efficiency[25], we attribute the gap to be noise, limited read power and the mode mismatch of coupling Stokes and anti-Stokes photons. Another individual high-intensity pulse generator is needed to enable controlling the moment, frequency, bandwidth and intensity of the write and read pulse separately, which make it possible to optimise one without disturbing the other. As to memory retrieval efficiency itself, further improvement includes shaping the read pulse [37], retrieval in backward direction [38] and cavity enhancement[39].

Although the time bandwidth product has already been very high, the longer absolute lifetime means fewer quantum repeater nodes for a given quantum communication distance[7,

32]. The dominant factor of decoherence mechanism in our current setup is motion induced loss, which may be solved by using a small-diameter cell to keep atoms always staying in the interaction region. Meanwhile anti-relaxation coating should be adopted to keep atomic polarisation during its collision with cell. The lifetimes of Zeeman populations and coherences in excess of 60 seconds has been reported [40], making it promising with large space for realising longer storage lifetime.

In summary, we have demonstrated a broadband DLCZ quantum memory in room-temperature atoms. Low unconditional noise level, strong nonclassicality preserved among heralding photon and stored excitation, and large time bandwidth product and ability of operating at room temperature make far-off resonance DLCZ quantum memory promising for future scalable quantum technologies [1], and promptly applicable in building large-scale quantum networks [41].

Methods

Programmable generation of high-intensity write/read pulse: Far-off resonance DLCZ quantum memory requires broadband and high-intensity write/read pulse. We cannot generate it directly from a high-power continuous laser since the required peak power exceeds the threshold of fast Electro Optic Modulator (EOM). A customised commercial Ti:sapphire laser may provide required bandwidth and intensity. However, fixed periodic generation of pulse means incapability to write and read on-demand, resulting in inadequate exploitation of time bandwidth product of quantum memory. We develop a system to generate high-intensity pulse with tunable central frequency, bandwidth, and more importantly, generation time. An external cavity diode laser (ECDL) locked to the transition $6S_{1/2}, F = 4 \rightarrow 6S_{3/2}, F' = 4\,\mathrm{co}\,5$ line of caesium serves as reference called MASTER. Another distributed Bragg reflector (DBR) laser called SLAVE are locked to MASTER in an arbitrarily set frequency difference by comparing their frequency on a Fabry-Perot etalon. A fast EOM trigged by electronic pulses from field-programmable gate array (FPGA) is used to chop SLAVE to short pulses. The generated pulses are fed into a homemade tapered amplifier (TA) to boost their power by 17 dB. In order to eliminate the spontaneous emission from the TA, we employ a ruled diffraction grating to spread beam out and spatially pick the stimulated radiation with irises. In our experiment, full width at half maximum (FWHM) of the write/read pulse is 2.3 ns, measured by a fast photodiode whose rise time is tens of picoseconds. Their pulse profile can be fitted by a Gaussian function with a FWHM of 2.206 ns, corresponding to a bandwidth of 200 MHz.

Cascaded cavities filter: Collinear configuration of writing and reading offers longer spin wave lifetime while makes single photons very hard to filtered out of strong addressing light. We develop two sets of cascaded cavities composed of three Fabry-Perot cavities tuned resonant with Stokes and anti Stokes respectively. Every cavity is a monolithic plank-convex glass. Both sides are coated to give a transmission window FWHM about 380 MHz. Careful alignment is necessary to optimise mode matching between cavity and incident light, which determines the performance in terms of transmission and extinction ratio. The transmission frequency can be tuned by setting the temperature of the cavity. We use an active feedback system to set the temperature and also lock it within $\pm\,3$ mK. For each cavity, we obtain a transmission rate of more than 90% and an extinction ratio of more than 500. With three cavities together we have a transmission rate over 70% and total extinction ratio up to 10^7.

Convolution-based bandwidth measurement: As shown in Figure 3a and 3d, the transmission profiles of Stokes and anti-Stokes through cascaded cavities are fitted by using

$$T(f) = \frac{T_0}{1 + A\sin^2\left[d\left(f - f_0\right)\right]} \cdot \frac{1}{1 + B\sin^2\left[h\left(f - f_0\right)\right]} \cdot \frac{1}{1 + C\sin^2\left[g\left(f - f_0\right)\right]} \tag{3}$$

where T_0, A, B, C, d, h, g and f_0 are fitting parameters. Frequency difference refers to $f - f_0$. The grey circles are experimental data and the green lines are fitting curves. Figure 3b and 3e are fitted by using

$$U(f) = a\exp\left[\frac{-2\left(f - b\right)^2}{d^2}\right] + U_0, \tag{4}$$

where a, b, d and U_0 are fitting parameters. The grey columns are experimental data and the blue lines are fitting curves. It is reasonable to consider U_0 as noise rather than signal photons, so it is $U(f) - U_0$ rather than $U(f)$ that describes real convolutions. If function $S(f)$ is assumed to be the frequency spectra of Stokes photons or anti-Stokes photons, then

$$U(f) - U_0 = T(f) * S(f), \tag{5}$$

Applying convolution theorem, we achieve

$$F\{S(f)\} = \frac{F\{U(f) - U_0\}}{F\{T(f)\}}, \tag{6}$$

where $F\{S(f)\}$ is the Fourier transform of $S(f)$, similarly for $F\{U(f) - U_0\}$ and $F\{T(f)\}$. By applying inverse Fourier transform to $F\{S(f)\}$, we derive out the spectrum $S(f)$ of Stokes photons or anti-Stokes photons. The spectra are shown in Figure 3c and 3f.

Acknowledgements: The authors thank J.-W. Pan and H.-J. Li for helpful discussions. This research leading to the results reported here was supported by the National Natural Science Foundation of China (No.11374211), the Innovation Program of Shanghai Municipal Education Commission (No.14ZZ020), Shanghai Science and Technology Development Funds (No.15QA1402200), and the open fund from HPCL (No.201511-01). X.-M.J. acknowledges support from the National Young 1000 Talents Plan.

[1] O'Brien, J. L., Furusawa, A. & Vučković, J. Photonic quantum technologies. *Nature Photon*. **3**, 687-695 (2009).

[2] Jin, X. -M. *et al.* Experimental Free-Space Quantum Teleportation. *Nature Photon.* **4**, 376-381 (2010).

[3] Gisin, N. & Thew R. Quantum communication. *Nature Photon*. **1**, 165-171 (2007).

[4] Ladd, T. D. *et al.* Quantum computers. *Nature* **464**, 45-53 (2010).

[5] Aspuru-Guzik, A. & Walther, P. Photonic quantum simulators. *Nature Phys*. **8**, 285-291 (2012).

[6] Lvovsky, A. I., Sanders, B. C. & Tittel, W. Optical quantum memory. *Nature Photon*. **3**,706-714 (2009).

[7] Briegel, H.-J., Dür, W., Cirac, J. I. & Zoller, P. Quantum repeaters: The role of imperfect local operations in quantum communication. *Phys. Rev. Lett.* **81**, 5932-5935 (1998).

[8] Duan, L. -M., Lukin, M. D., Cirac, J. I. & Zoller, P. Long-distance quantum communication with atomic ensembles and linear optics. *Nature* **414**, 413-418 (2001).

[9] Nunn, J. *et al.* Enhancing Multiphoton Rates with Quantum Memories. *Phys. Rev. Lett.* **110**, 133601 (2013).

[10] Chanelière, T. *et al.* Storage and retrieval of single photons transmitted between remote quantum memories. *Nature* **438**, 833-836 (2005).

[11] Eisaman, M. D. *et al.* Electromagnetically induced transparency with tunable single-photon pulses. *Nature* **438**, 837-841 (2005).

[12] Zhang, H. *et al.* Preparation and storage of frequency-uncorrelated entangled photons from cavity-enhanced spontaneous parametric downconversion. *Nature Photon.* **5**, 628-632 (2011).

[13] Kuzmich, A. *et al.* Generation of nonclassical photon pairs for scalable quantum communication with atomic ensembles. *Nature* **423**, 731-734 (2003).

[14] Julsgaard, B., Kozhekin, A. & Polzik, E. S. Experimental long-lived entanglement of two macroscopic objects. *Nature* **413**, 400-403 (2001).

[15] Julsgaard, B., Sherson, J., Cirac, J. I., Fiuŕašek, J. & Polzik, E. S. Experimental demonstration of quantum memory for light. *Nature* **432**, 482-486 (2004).

[16] Moiseev, S. A. & Kröll, S. Complete reconstruction of the quantum state of a single-photon wave packet absorbed by a Doppler-broadened transition. *Phys. Rev. Lett.* **87**, 173601 (2001).

[17] Kraus, B. *et al.* Quantum memory for nonstationary light fields based on controlled reversible inhomogeneous broadening. *Phys. Rev. A* **73**, 020302(R) (2006).

[18] Alexander, A. L., Longdell, J. J., Sellars, M. J. & Manson, N. B. Photon echoes produced by switching electric fields. *Phys. Rev. Lett.* **96**, 043602 (2006).

[19] Tittel, W. *et al.* Photon-echo quantum memory in solid state systems. *Laser Photon. Rev.* **4**, 244-267 (2010).

[20] Afzelius, M., Simon, C., de Riedmatten, H. & Gisin, N. Multimode quantum memory based on atomic frequency combs. *Phys. Rev. A* **79**, 052329 (2009).

[21] Buchler, B. C., Hosseini, M., Hétet, G., Sparkes, B. M. & Lam, P. K. Precision spectral manipulation of optical pulses using a coherent photon echo memory. *Opt. Lett.* **35**, 1091-1093 (2010).

[22] Hosseini, M., Sparkes, B. M., Campbell, G., Lam, P. K. & Buchler, B. C. High efficiency coherent optical memory with warm rubidium vapour. *Nature Commun.* **2**, 174 (2011).

[23] Liao, W. -T., Keitel, C. H., and Pálffy, A. All-Electromagnetic Control of Broadband Quantum Excitations Using Gradient Photon Echoes. *Phys. Rev. Lett.* **113**, 123602 (2014).

[24] Reim, K. F. *et al.* Towards high-speed optical quantum memories. *Nature Photon.* **4**, 218-221 (2010).

[25] Reim, K. F. *et al.* Multi-pulse addressing of a Raman quantum memory: configurable beam splitting and efficient readout. *Phys. Rev. Lett.* **108**, 263602 (2012).

[26] Ding, D.-S. *et al.* Raman quantum memory of photonic polarized entanglement. *Nature Photon.* **9**, 332-338 (2015).

[27] Manz, S., Fernholz, T., Schmiedmayer, J., Pan, J.-W. Collisional decoherence during writing and reading quantum states. *Phys. Rev. A* **75**, 040101(R) (2007).

[28] Michelberger, P. S.*et al.* Interfacing GHz-bandwidth heralded single photons with a warm vapour Raman memory. *New J. Phys.* **17**, 043006 (2015).

[29] Lee, K. C. *et al.* Entangling macroscopic diamonds at room temperature. *Science* **334**, 1253-1256 (2011).

[30] England,D. G. *et al.* Storage and Retrieval of THz-Bandwidth Single Photons Using a Room-Temperature Diamond Quantum Memory. *Phys. Rev. Lett.* **114**, 053602 (2015).

[31] Clauser, J. F. Experimental distinction between the quantum and classical field-theoretic predictions for the photoelectric effect. *Phys. Rev. D* **9**, 853-860 (1974).

[32] Sangouard, N., Simon, C., de Riedmatten, H., Gisin, N. Quantum repeaters based on atomic ensembles and linear optics. *Rev. Mod. Phys.* **83** 33-80 (2011).

[33] Duan, L. -M., Cirac, J. I. & Zoller, P. Three-dimensional theory for interaction between atomic ensembles and free-space light. *Phys. Rev. A* **66**, 023818 (2002).

[34] Zhao, B. *et al.* A millisecond quantum memory for scalable quantum networks. *Nature Phys.* **5**, 95-99 (2009).

[35] Nunn, J. Quantum Memory in Atomic Ensembles. Ph.D. thesis, University of Oxford, 481-487 (2008).

[36] Bashkansky, M., Fatemi, F. K. and Vurgaftman, I. Quantum memory in warm rubidium vapor with buffer gas. *Opt. Lett.* **37**, 142-144 (2012).

[37] Novikova, I., Phillips, N. B. & Gorshkov, A. V. Optimal light storage with full pulse-shape control. *Phys. Rev. A* **78**, 021802(R) (2008).

[38] Surmacz, K. *et al*. Efficient spatially resolved multimode quantum memory. *Phys. Rev. A* **78**, 033806 (2008).

[39] Nunn, J. *et al.* Theory of noise suppression in Λ-type quantum memories by means of a cavity. *arXiv*:1601.00157 (2016).

[40] Balabas, M.V., Karaulanov, T., Ledbetter, M. P. & Budker, D. Polarized Alkali-Metal Vapor with Minute-Long Transverse Spin-Relaxation Time. *Phys. Rev. Lett.* **105**, 070801 (2010).

[41] Kimble, H. J. The quantum internet. *Nature* **453**, 1023-1030 (2008).